

VIBRATION LOADS PREDICTION IN THE AGE OF CFD

Oliver Dieterich Peter Konstanzer Markus Dietz
Oliver.dieterich@eurocopter.com, Peter.konstanzer@eurocopter.com, Markus.dietz@eurocopter.com
 Eurocopter Deutschland GmbH, D-81663 Munich, Germany

Abstract

During the last decade, we have seen a successful transfer of computational fluid dynamics (CFD) applications on rotor and rotorcraft systems from academic examples to – from industrial point of view – more product oriented cases putting a significant step forward to the usage of more advanced methods for design purposes. Nevertheless, main focus – while performing CFD – is still put on aerodynamics characteristics although in the meantime a large variety of CFD solvers are coupled to structural dynamic solvers allowing to take into account rotor aero-elasticity or even rotor aero-servo-elasticity. On the other hand, it is well known that the predictive capabilities with respect to vibratory rotor loads and vibrations are still considered inadequate in general for industrial needs. Therefore, natural expectations exist that the application of CFD will also lead to quantitative improvements in the analysis of vibratory rotor loads and vibrations. As a step in this direction, this paper is dedicated to the comparison and assessment of vibratory blade loads from flight test with numerical results obtained by both CFD and conventional methods. Furthermore, the impact of boundary conditions typically applied to that kind of prediction models will be analysed in the paper.

1. INTRODUCTION

The prediction of vibratory loads and vibrations for rotorcraft applications is still a challenging and for industrial purposes highly important task. Looking on today's comprehensive rotor codes and their application e.g. models featuring elastic beams, lifting line theory and advanced wake models, the prediction capabilities are still not fully satisfying for industry needs [1, 2]. The open question now is to which extent the application of CFD might help closing the gap between the urgent industrial requirements on the one hand and the potential offered by advanced CFD methods on the other hand.

In the rotorcraft community it is well acknowledged that during the last decade, CFD has proven to be an efficient and reliable means for improving aerodynamic predictions and analysis for rotorcrafts and rotor systems. Furthermore, the progress in computer hardware and in efficient calculation schemes has paved the way for using CFD tools in industrial environments and for complex design purposes [3]. While rotorcraft CFD applications of the first generation were related to 'pure' aerodynamic issues, state-of-the-art CFD solutions have been coupled in the meantime to aeroelastic rotor models allowing to

answer also questions from aeroelastics and dynamics point of view.

In [4], an industrial approach has been presented regarding the usage of aeroelastic rotor CFD for answering fundamental aerodynamic questions. The approach was based on a weak coupling methodology between CFD and comprehensive rotor codes. In this paper, a comparison between numerical and flight test results was presented with focus on rotor performance and overall blade loads for a BK117 C-1 equipped with an experimental four-bladed hingeless main rotor system.

In this paper, the work is extended with respect to vibrations and vibratory loads. For the four-bladed rotor of the test vehicle, 3/rev, 4/rev and 5/rev vibratory blade loads are of special interest for dynamics. The flap moments lead to vibratory 4/rev hub pitch and roll moments while related shear and axial forces at the blade roots generate 4/rev rotor thrust and in-plane forces. Blade load signals from the flight tests are compared to those of the coupled CFD solution. In addition, free wake models are also applied in order to allow assessing the benefits of CFD for vibration prediction accuracy in the view of industrial requirements.

Reviewing the numerical model, aeroelastic analysis of rotor systems is often treated using isolated rotor models fixed to ground as it was the case in [4]. Roll and pitch attitude are taken into account by adequate rotor shaft orientation and rotor trim is performed for non-articulated rotors respecting rotor thrust and hub moments. The open issue is whether especially for the prediction of higher harmonic rotor loads this modelling approach is still sufficient in terms of accuracy. From aerodynamics point of view, interference effects of the fuselage modifying the inflow conditions of the rotor disk might play a significant role. From structural dynamic point of view, coupling phenomena affect rotor response with respect to the drive train system and the rotor support. Therefore, approaches for improving the rotor model for vibratory loads prediction are presented with focus on structural dynamic modelling.

2. TEST CASE DEFINITION

2.1. Flight Test Database

As already presented in [4], the test case chosen for the coupled computations is a four-bladed experimental hingeless rotor – featuring a Boelkow rotor hub and exchangeable blade tips – in steady forward flight condition at 135 KTAS. The rotor system was tested on the BK117 helicopter. The experimental test bed is shown in Figure 1.



Figure 1: BK117 experimental test bed
(© Eurocopter Deutschland GmbH)

Regarding the numerical investigations, the main rotor was trimmed to thrust, roll and pitch moment using collective and cyclic controls. While rotor pitch and roll moments were measured during flight test and are thus directly usable for trimming the rotor thrust is not directly available from experimental data. In order to provide a realistic value for rotor thrust a complete helicopter trim computation had been performed with an in-house flight mechanics code. In order to complete adequate operating conditions for the rotor model, the rotor orientation was

chosen in agreement to rotorcraft pitch and roll attitude with respect to the wind axes and inertial frames.

An extract of the rotor flight condition and the trim objectives is listed in Table 1.

True Air Speed	135 kts
Rotor advance ratio	0.31
Flight speed Mach number	0.206
Blade tip Mach number	0.661
Rotor shaft pitch angle	-6.0°
Rotor shaft roll angle	+0.2°
Thrust coefficient (derived from flight mechanics computation)	0.0071
Rotor hub pitch moment coefficient (from flight test)	8.52×10^{-5}
Rotor hub roll moment coefficient (from flight test)	7.48×10^{-6}

Table 1: Flight condition and trim objective

For the comparison of flight test data with the numerical models, the following main rotor blade load data measured by strain gauges were selected for this paper:

Flap bending:

- MB3410: $r = 3410 \text{ mm}$, $r/R = 0.620$

Lag bending:

- MZ1210: $r = 1210 \text{ mm}$, $r/R = 0.220$

Blade torsion:

- MT1290: $r = 1662 \text{ mm}$, $r/R = 0.302$

In this context it should be mentioned that the main rotor blades feature pendulum absorbers in the blade neck area in order to reduce the vibratory hub loads. Thus, the consideration of blade pendulum absorbers in the structural dynamic models is of high importance especially in view of comparing higher harmonic inboard blade flapping moments.

2.2. Numerical Model Setup

Details of the CFD solver, the structural dynamic models and the weak coupling procedures for the main rotor system are described in detail in [4]. As CFD tool, the FLOWer code developed by DLR [5] was applied. The blade meshes were based on a multi-block topology with C-type topology in chordwise direction and O-type topology in spanwise direction. Table 2 summarizes the grid data of the related Chimera system. The complete grid system consists of roughly 8 million grid cells.

Grid	Number of blocks	Number of cells
Blade grid	4 x 30	1,750,016
Background grid	4	1,327,104
Total	124	8,327,168

Table 2: CFD grid data

Special care was given on the rotor modelling in view of the flight tests. Trailing edge tabs were included in the CFD mesh in order to take into account their impact on aerodynamic loads especially torsion moments.

In [4], two different structural dynamic solvers were applied to the test case: one emanated from the commercial code CAMRAD II [6] and one implemented in the EUROCOPTER in-house tool HOST [7]. Both codes use a beam model approach for representing blade structural dynamics. Furthermore, both codes are linked to the CFD solver by a weak coupling approach with some slight differences. While the air loads are exchanged by discrete loads for CAMRAD II, the HOST code refers to aerodynamic line loads allowing additional flexibility in the different discretization schemes.

3. BASELINE RESULTS

This section presents the blade loads results for the isolated CAMRAD II rotor model. Major physical approximations for the structural dynamic model are seen in the prescribed main rotor shaft rotation neglecting any drive train and rotor shaft dynamics and in the rigid main rotor support neglecting any kind of vibrations coming from the airframe. Regarding aerodynamics, the role of aerodynamics interference from the airframe was already demonstrated in [4]. In the present studies, no interference effects are taken into account.

Figure 2 to Figure 4 present the histories of the trim settings for the main rotor trim during the weak coupling procedure. An azimuth range of 135 deg was processed by the CFD solver for each weak coupling iteration step. The figures start with iteration 5 as some minor model changes were introduced at this step. Although these model modifications generated some perturbations visible by the differences between iterations 5 and 6, the coupled model settled down quite fast in the following iterations.

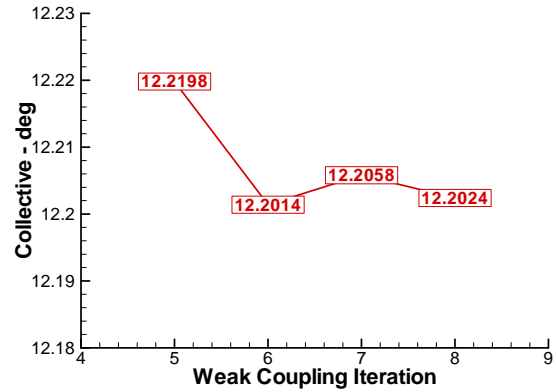


Figure 2: Trim history collective setting

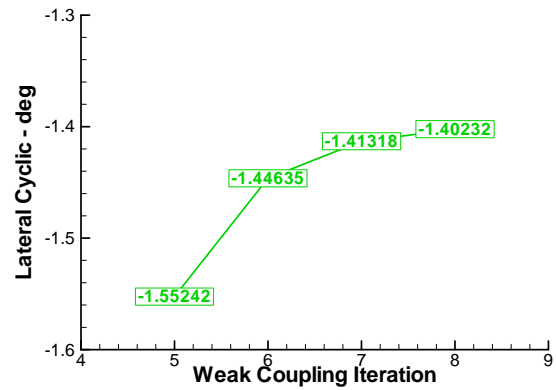


Figure 3: Trim history lateral cyclic setting

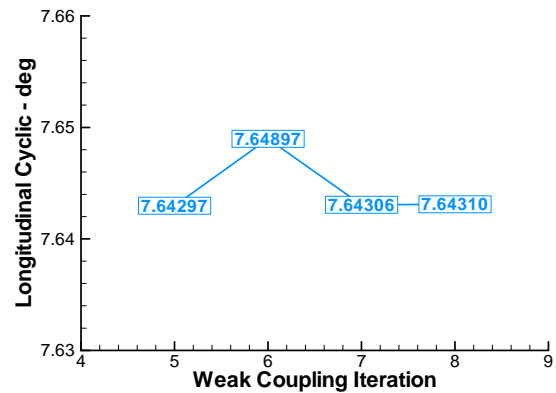


Figure 4: Trim history longitudinal cyclic setting

For analysis of the harmonic contents of the numerical model response, a pre-requisite in terms of convergence consists in the stationarity of the harmonics. Thus – as next step – the harmonics of the various iterations are plotted for blade flap and lag bending moments as well as for the blade torsion moment. Figure 5 shows the response of the first up to the fifth harmonics for the flap bending moment sensor MB3410 in a polar plot. A logarithmic amplitude axis was engaged in order to cover the large range of amplitudes for the envisaged range of harmonics. As already mentioned above the harmonics 1 to 5 are of high interest for vibration assessment

especially harmonics 3 to 5 for this four-bladed main rotor. In the following the harmonics in the plots are coded by both symbol shape and colour. As shown in the legend, the first harmonic is marked by a red circle, the second one by a green square, the third one by a blue gradient operator symbol, the fourth one by a grey diamond and the fifth one by an orange delta symbol.

In order to track the trim iterations, iteration 5 is labelled by hollow symbols while the two last iterations 7 and 8 are marked by a filled symbol and a black dot in order to monitor related changes. As clearly visible in Figure 5 by the centered dots, the harmonics can be considered stationary with respect to the last two iterations. Thus the weak coupling procedure is considered as adequately converged for harmonics analysis – at least up to the fifth harmonic. Figure 6 and Figure 7 present the related results for blade lag and torsion moments. In general the conclusions drawn for the blade flap bending moments are also confirmed for lag and – showing some minor offsets – for torsion.

4. COMPARISON WITH FLIGHT TEST DATA

As next step, the numerical results of the coupled solution will be compared with flight test data. In this context it should be mentioned that the data acquisition procedure of experimental data needs adequate consideration especially in case of the higher harmonics potentially experiencing significant phase delays. In the following figures which are organised in a similar way as before, the flight test data points are shown as black filled symbols while iteration 8 as last weak coupling iteration representing the numerical data is shown by coloured symbols. In order to facilitate the overview the relationship of flight test data point to numerical data point is highlighted by dashed lines.

For the blade flapping moments plotted in Figure 8, the order of magnitudes seems more or less correctly calculated but significant phase deviations are visible. Obviously the higher the harmonic number, the higher the deviation which is in line with the general experience that the higher the frequencies the less accurate the numerical models.

MB3410
Isolated Rotor

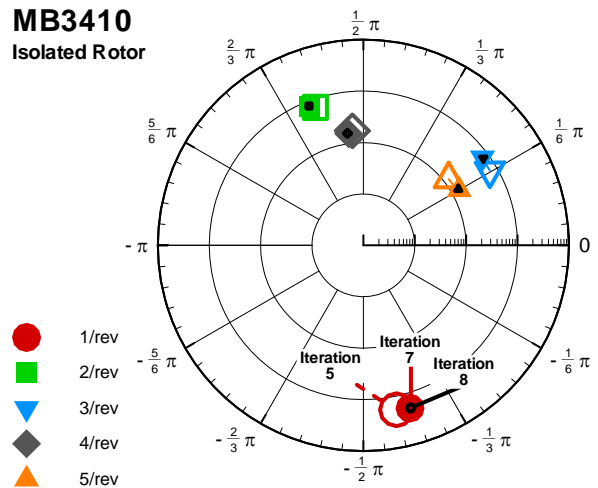


Figure 5: Trim history of blade flap bending moment MB3410

MZ1210
Isolated Rotor

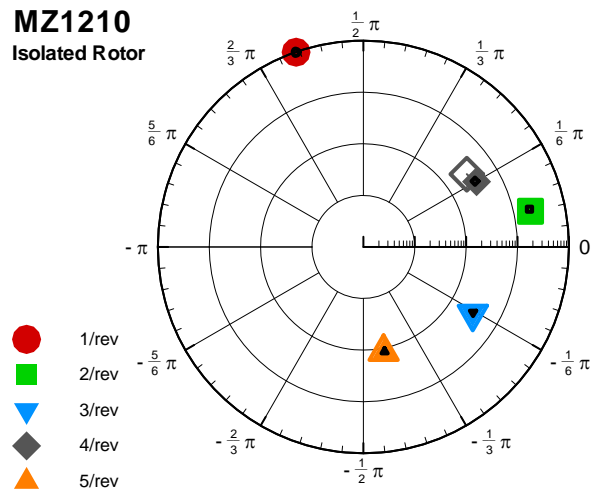


Figure 6: Trim history of blade lag bending moment MZ1210

MT1290
Isolated Rotor

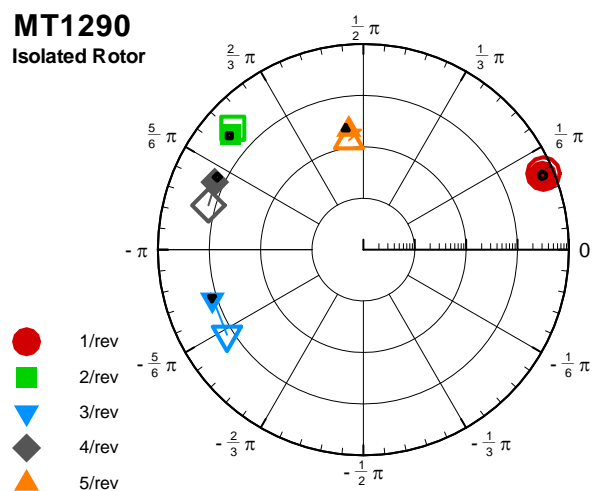


Figure 7: Trim history of blade torsion moment MT1290

Regarding the blade lag moments shown in Figure 9, the orders of magnitude are less accurate visible by the dashed lines changing radii. Furthermore, a phase shift of approximately 180 deg is noticed for the blade passage frequency expected to be related to the missing drive train model. Please remind that for the isolated rotor model the rotor shaft rotation is constraint by a constant rotor speed which can be compared to the boundary condition of a clamped beam.

Figure 10 presents the blade torsion moments. In general the agreement is acceptable with the exception of the phase difference for the third harmonic. It is assumed that similar to Figure 9 a principal modelling issue is responsible for this behaviour. A potential uncertainty source is seen in the simplified modelling approach for the pitch control system including its flexibilities.

5. COMPARISON WITH FREE WAKE MODELS

In order to assess the benefits of CFD, free wake calculations corresponding to those presented in [4] are studied in a similar manner. In the following figures, flight test results are again shown as black filled symbols – as well as the coupled solution as coloured filled symbols – while the free wake results are plotted using hollow coloured symbols. No differences were made between the four wake models for demonstration purposes.

Figure 11 shows the free wake results for the blade flap bending moments in comparison to flight tests and to the coupled (CFD) solution. Although no metrics have been defined in this paper for the rating of the models one gets the impression that in general the coupled results are ‘closer’ to the flight tests than the free wake models.

In Figure 12, the situation seems not so obvious for the lag bending moments. The benefits from CFD show a more pronounced impact on blade flap moments than on blade lag moments for the selected sensors. This behaviour is to some extent expected as aerodynamic drag forces mainly affecting blade lagging are orders of magnitude smaller than aerodynamic lift forces affecting mainly blade flapping. A still unresolved issue is the deviation of the phase of the fourth harmonic.

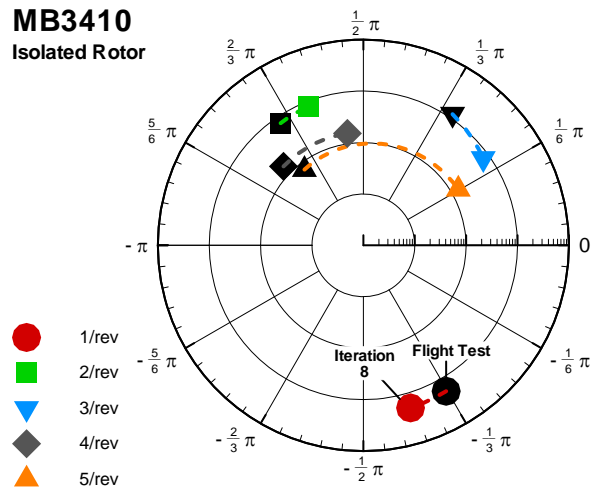


Figure 8: Comparison flight test versus coupled solution MB3410

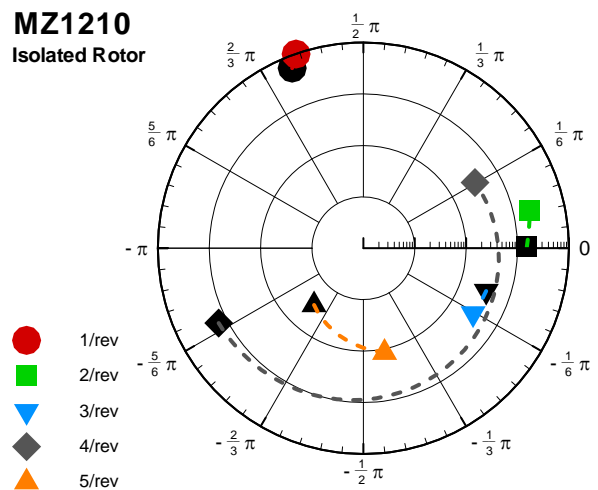


Figure 9: Comparison flight test versus coupled solution MZ1210

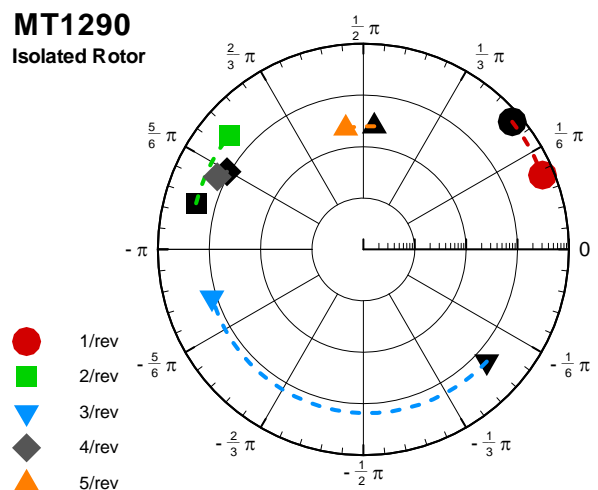


Figure 10: Comparison flight test versus coupled solution MT1290

MB3410

Isolated Rotor

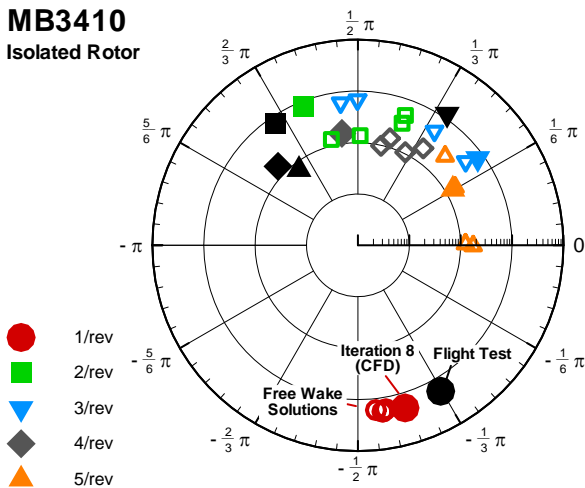


Figure 11: Comparison with free wake models MB3410

MZ1210

Isolated Rotor

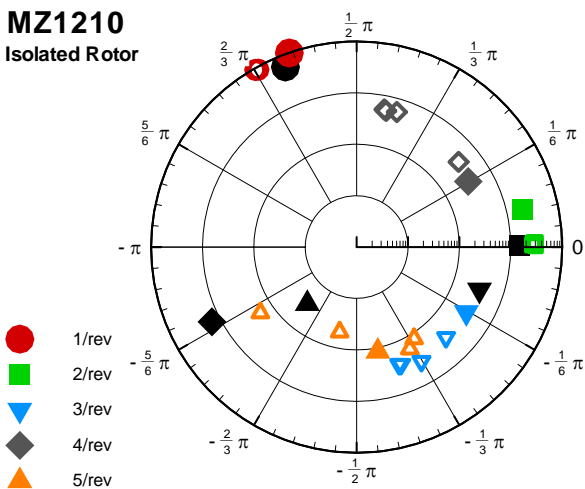


Figure 12: Comparison with free wake models MZ1210

MT1290

Isolated Rotor

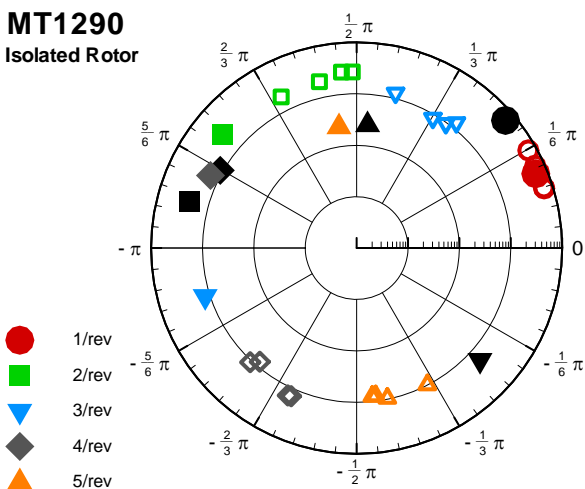


Figure 13: Comparison with free wake models MT1290

In order to complete the view, Figure 13 presents the blade torsion moments. The behaviour seen here resembles more to that of the blade flap moments demonstrating a clear benefit of the CFD. It should be added that the phase deviation of the third harmonic could not be improved in magnitude but directions changed.

6. INCLUSION OF DRIVE TRAIN MODEL

As next step, the boundary condition of prescribed rotor rotation is released by the implementation of a simplified drive train model introducing a rotational rigid body degree of freedom for the drive train system and elastic shaft rotations for both rotor and engine shaft. Thus, the rotation speed of the rotor is depending on the rotor azimuth. In case of a perfect rotor with identical blades, as assumed here, the rotation speed – as part of the structural dynamic solution process – will vary at blade passage frequency and integer multiples of it. Thus, changes in the blade load responses are especially expected for the fourth harmonics in the related figures.

In the current development step, the drive train model was only introduced on the structural dynamic solver side. The rotor speed variations have been checked with respect to the hereby neglected variations of blade tip speed variations. The perturbations were found to be of negligible impact on CFD solver side.

The drive train model was implemented starting with iteration 8d – label d introduced for drive train model. The isolated rotor model of iteration 7 was used for initialisation of the coupled analysis on both CFD and structural dynamic solver sides. Results of three iterations 8d, 9d and 10d are available each of them based again on 135 deg azimuth range for the CFD solver. The trim histories showing the impact of the drive train model on collective and cyclic settings are shown in Figure 14 to Figure 16 using the same scales as in Figure 2 to Figure 4. Again, the impact of the model change on main rotor trim levelled out quite fast.

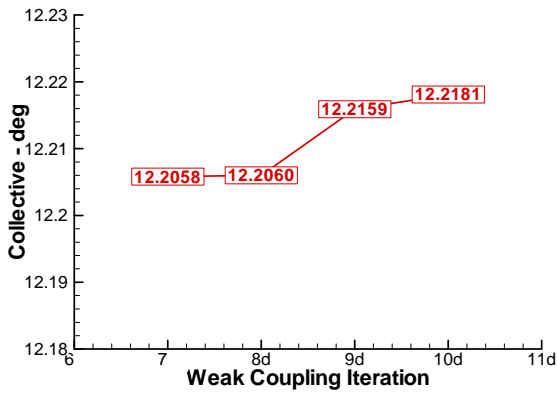


Figure 14: Trim history for model with drive train: collective

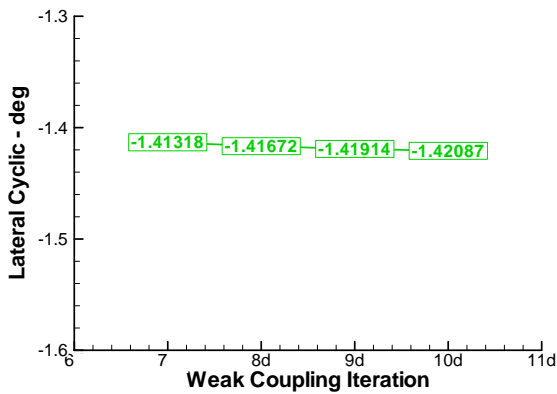


Figure 15: Trim history for model with drive train: lateral cyclic

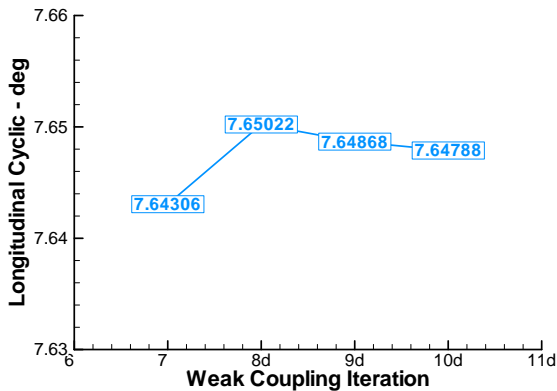


Figure 16: Trim history for model with drive train: longitudinal cyclic

Figure 17 to Figure 19 show the changes in the harmonics obtained by the inclusion of the drive train model. Flight test data points are plotted in black filled symbols, isolated rotor results in coloured hollow symbols and the coupled rotor-drive train models in coloured filled symbols. Regarding the blade flap moments presented in Figure 17 almost no visible changes are noted for the first and second harmonic. The third and fifth harmonic show slight improvements comparing the coloured symbols,

while the fourth harmonic does not. Interestingly, changes are not restricted to the fourth harmonic.

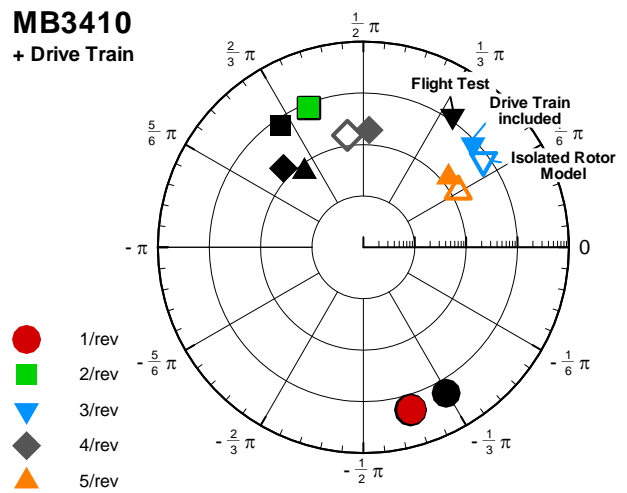


Figure 17: Comparison with drive train model MB3410

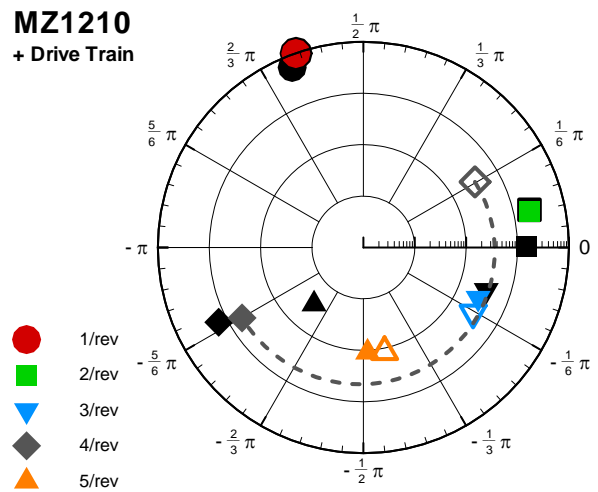


Figure 18: Comparison with drive train model MZ1210

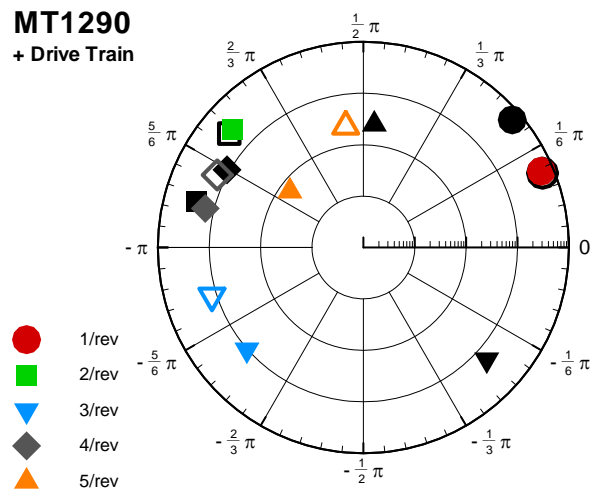


Figure 19: Comparison with drive train model MT1290

As expected, Figure 18 offers more significant differences. While slight changes are noted again for the third and fifth harmonic, the phase of the fourth harmonic is now changed by almost 180 deg leading to a noticeable agreement with the flight test data. For highlighting this issue the phase change of the fourth harmonic is plotted in the figure by a dashed grey line. Nevertheless, it also has to be mentioned that a significant amplitude deviation for the fourth harmonic is still visible. Again, the impact on first and second harmonic is negligible.

Compared to the other results considering the drive train model, the torsion moments plotted in Figure 19 behave more indifferent. Slight degradations are seen for the fourth and fifth harmonics while first and second harmonics are still very stationary. The third harmonic could only be slightly improved with respect to the large phase error.

7. INCLUSION OF AIRFRAME MODEL

In addition to the drive train model, an airframe model was implemented as natural subsequent step introducing additional degrees of freedom for rigid body motions as well as elastic airframe modes. Thus, the rotor is undergoing motions – translations and rotations – with respect to the inertial frame. Taking into account the mechanical filtering properties of an ideal rotor with identical blades, see also the remarks for the drive train model, the airframe degrees of freedom are expected to respond at blade passage frequency and integer multiples of it. Similar to the rotor model coupled with the drive train, the impact of the moving rotor support on the CFD part is neglected at the moment. Figure 23 gives an impression of the airframe model used for the calculation of the modal properties. Due to the considerable age of the Finite Element model, a quite coarse mesh is visible which does not match today’s standards in model accuracy. Nevertheless, for analysing the impact of the airframe on rotor loads in general, it is expected to allow the drawing of adequate conclusions.

The airframe model was introduced starting with iteration 10 – as shown by label a for the iteration step in Figure 20 to Figure 22. Again each iteration applied the CFD solver for an azimuth range of 135 deg.

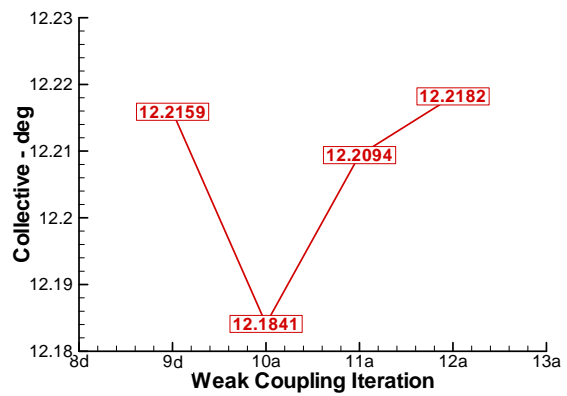


Figure 20: Trim history for model with airframe: collective

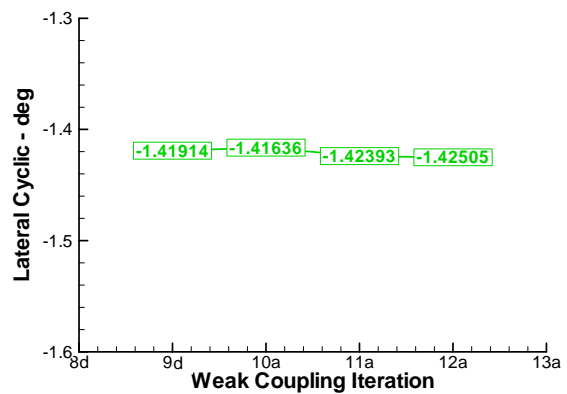


Figure 21: Trim history for model with airframe: lateral cyclic

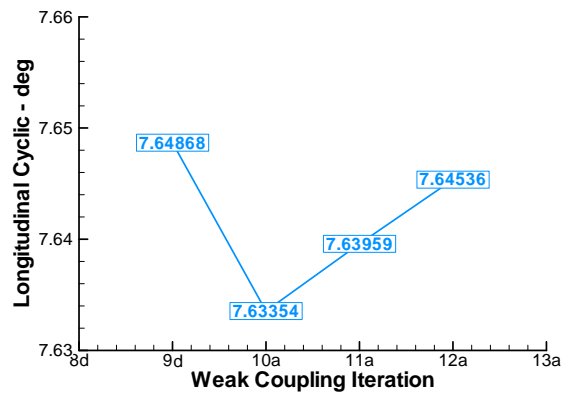


Figure 22: Trim history for model with airframe: longitudinal cyclic



Figure 23: Finite Element airframe model of BK117

MB3410
+ Airframe

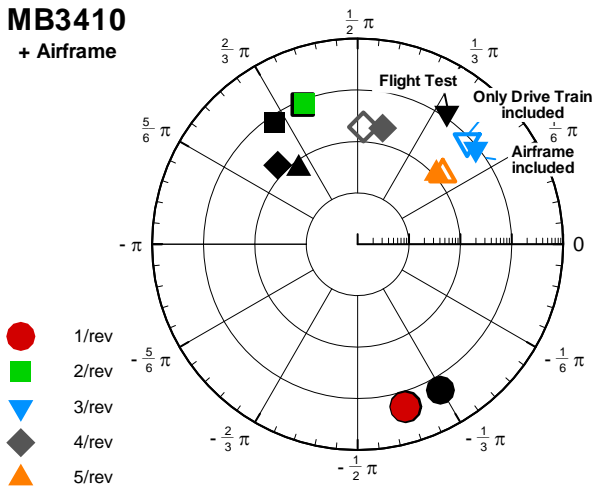


Figure 24: Comparison with airframe model MB3410

MZ1210
+ Airframe

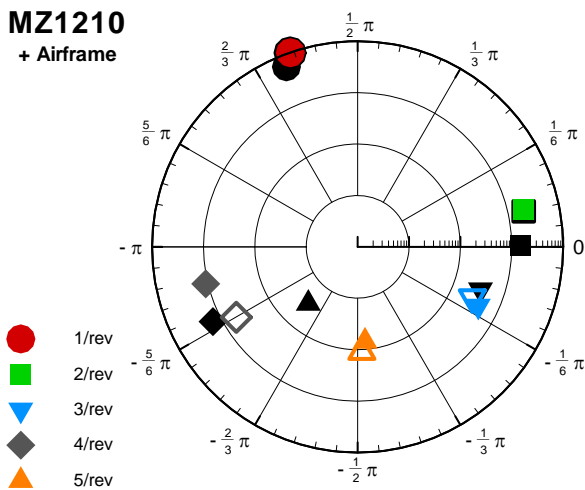


Figure 25: Comparison with airframe model MZ1210

MT1290
+ Airframe

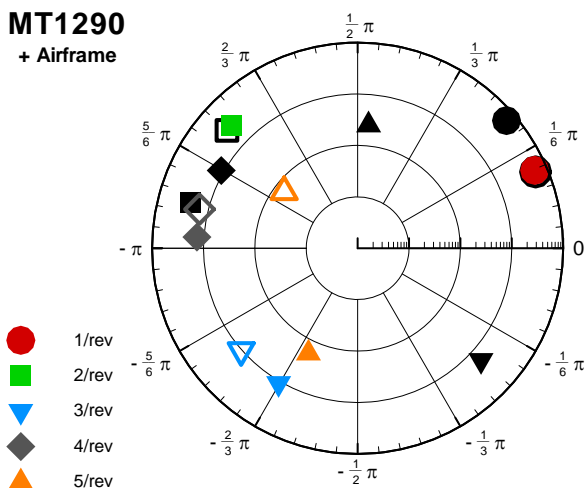


Figure 26: Comparison with airframe model MT1290

As the airframe model is added to the rotor model with drive train, comparisons of the airframe model results in the figures are performed versus flight tests on the one hand and versus the drive train model on the other hand. As usual, flight tests are labelled by black symbols. This time the coloured hollow symbols are related to rotor model with drive train while the coloured filled symbols present the results with both airframe and drive train models included. Similar to the drive train model, changes are mainly visible for the harmonics 3 to 5. In Figure 24 a slight degradation especially in phase is noted for the related flap bending moments. In Figure 25, the amplitudes of the harmonics 3 to 5 are shifted in the correct directions while the phases are also slightly degraded. Figure 26 shows the results for the torsion moment with different trends for the harmonics.

Concluding the figures which show the impact of the airframe model, the results are not fully convincing. Potential for improvements is especially seen in a more accurate Finite Element model of the airframe. Still today, it is a challenging task to set up a Finite Element model of a rotorcraft airframe adequately accurate for higher frequencies.

8. CONCLUSIONS

Despite the progress achieved in aeromechanics tools development during the last decades, vibratory rotor and blade load prediction of today based on conventional models is still not fully satisfying in terms of accuracy. This paper shows that for the chosen test case of a BK117 equipped with a four bladed hingeless main rotor, significant improvements are visible in the calculation of blade bending and torsion moments by applying CFD coupled to aeroelastic models. Nevertheless, differences to flight test data are still visible for the isolated rotor model. Thus, CFD is judged to be an important step towards improved prediction capabilities for vibrations but it is not the only brick missing up to now in the wall of total breakthrough for vibration prediction.

Therefore, the role of structural dynamic interference with a drive train model and an airframe model was investigated as well. While the application of the drive train model improves in general the calculations, the results with respect to the airframe model are not so unique. For final statements, an improvement of the airframe model seems to be required. Furthermore, from structural dynamic point of view,

indications are noticed that a refinement of the control chain modelling might offer additional benefits.

This paper was focused on structural dynamic topics in the frame of vibratory load predictions. Starting with the isolated rotor model, structural dynamic components have been added towards a complete helicopter configuration. In a complementary way, it is expected that the consideration of fuselage aerodynamic interference effects will also lead to improvements in the calculations.

ACKNOWLEDGEMENTS

The authors would like to thank the German ministry of Economy and Technology (BMW) for its funding in the framework of MUSIHC.

REFERENCES

- [1] Bousman, W.G., Norman, T.R.: “*Assessment of predictive capability of aeromechanics methods*”, AHS Specialist’s Conference on Aeromechanics, San Francisco, CA, January 2008.
- [2] Johnson, W., Datta, A.: “*Requirements for next generation comprehensive analysis of rotorcraft*”, AHS Specialist’s Conference on Aeromechanics, San Francisco, CA, January 2008.
- [3] Dietz, M., Maucher, C., Schimke, D., „*Addressing today’s aeromechanic questions by industrial answers*“, AHS Specialist’s Conference on Aeromechanics, San Francisco, CA, January 2010.
- [4] Dietz, M., Dieterich, O., “*Towards increased industrial application of rotor aeroelastic CFD*”, Proceedings of the 35th European Rotorcraft Forum, Hamburg, Germany, September 2009.
- [5] Kroll, N., Eisfeld, B. and Bleecke, H.M., “*The Navier-Stokes Code FLOWer*”, Volume 71 of Notes on Numerical Fluid Mechanics, pages 58-71. Vieweg, Braunschweig, 1999.
- [6] Johnson, W.: “*Technology Drivers in the Development of CAMRAD II*“, AHS Specialist’s Conference on Aeromechanics, San Francisco, CA, January 1994.
- [7] Kampa, K., Benoit, B., Grünhagen, W.: “*HOST – a general helicopter simulation tool for Germany and France*”, Proceedings of the 56th HS Forum, Virginia Beach, USA; May 2000.